Journal of Fluid Science and Technology

Vol. 3, No. 3, 2008

Performance of Double-step Savonius Rotor for Environmentally Friendly Hydraulic Turbine*

Miyoshi NAKAJIMA**, Shouichiro IIO** and Toshihiko IKEDA**

**Department of Environmental Science and Technology, Shinshu University,
4-17-1 Wakasato, Nagano 380-8553, Japan.
E-mail: shouiio@shinshu-u.ac.jp

Abstract

The aim of this investigation is to develop an environmentally friendly nano-hydraulic turbine. Three type models of Savonius rotor are constructed and tested in a water tunnel to improve and clarify the power performance. Flow field around the rotor is examined visually to reveal the enhancement mechanisms of power coefficient using the double-step rotor. Flow visualization showed the difference of flow patterns at the central section between the standard (single-step) rotor and the double-step one. A meandering flow in the axial direction of the rotor was observed only for the double-step rotor. This flow had the pressure restoration effect at the returning blade's concave side and the torque strengthened effect at the advancing blade's convex side. As a consequence, the power coefficient was 10 % improved.

Key words: Environmentally Friendly Hydraulic Turbine, Savonius, Double-Step Rotor, Water Tunnel, Performance, Flow Visualization, Fluid Machinery

1. Introduction

Environmental issues as typified by global warming become conspicuous in recent years. It is obvious that achieving sustainable energy means using natural energy effectively. The hydropower should occupy the attention of electric power generating systems as it is clean and renewable energy sources with highest density, in cooperation with the wind and the solar powers. Most of hydropower is generated by the large-scale hydroelectric plant. Some have suggested that dam constructions can lead to the tremendous environmental damages. On the other hand, small/micro/nano hydropower has attracted much attention for recent years mainly because of decrease of construction place for large-scale plants and environmental conservation. The aim of this study is to develop a Savonius type hydraulic turbine to utilize effectively as the nano-hydropower and a dispersed power system. The turbine is suitable for the rivers or the irrigation canals in which the effective head is not sufficient while the flow rate is enough. It is thought that this approach could lead to cheaper power generation without the environmental disruptions, compared with that produced by large-scale hydroelectric plant.

Savonius rotor has been used mainly for a wind power [(1)-(20)] and tidal/wave power generation [(21)-(23)]. There have been many studies of Savonius rotor, e.g. rotor configurations [(1)-(3)], a flow field around a rotor [(4)-(6)], numerical simulations [(7),(8)], effect of guide vanes set around a rotor [(5),(9)-(14)] and others. Attempts have been made for the performance improvement of low-efficiency Savonius rotors by optimizing both rotor shape and wind collector.

The performance improvement of the Savonius rotors is an important challenge also in

*Received 3 Mar., 2008 (No. 08-0128)
[DOI: 10.1299/jfst.3.410]

this article for practical using of hydraulic turbines. So we first attempted to improve the efficiency by applying a phase difference to the blades of the Savonius rotor. This method is more conventional than installing guide vanes or others around the rotor, and is expected to improve the performance without losing the advantages of Savonius rotor, i.e. maintainability and economy. There are some reports [3],[15]~[20] on the power coefficient or torque performance of multi-step Savonius wind rotors with phase difference, but none of them have provided a detailed investigation on the effect of the blade's phase difference on the power performance from the flow field. In this article we aimed to clarify the effect of the phase difference in the blades of the Savonius rotor on the power performance and discuss in detail the improvement mechanism with double-step rotor from the visualization of the flow pattern around the rotor.

Nomenclature

A : projected area of rotor ($= D_R \cdot L_R$) [m^2]
C : overlap of blades [m]
C_P^* : power coefficient ($= P / {}^1/_2 \rho A U_0^3$)
D_B : chord of blade [m] (Fig. 3)
D_R : diameter of rotor [m] (Fig. 3)
H_0 : water level of water tunnel [m] (Fig. 2)
H_C : distance between rotor and bottom wall of water tunnel [m] (Fig. 2)
L_R : length of rotor [m] (Fig. 3)
N_T : rotational speed of rotor [rpm]
P : power output from rotor [W]
Re^* : Reynolds number ($= D_R \cdot U_0 / \nu$)
T : torque experienced by rotor [N・m]
U_0 : water velocity [m/s] (Fig. 2)
V_t : rotor tip speed [m/s]
λ^* : tip speed ratio ($= V_t / U_0$)
θ : angle of blade chord [deg.]
ν : kinetic viscosity of water [m^2/s]
ρ : water density [kg/m^3]
ω : angular velocity of rotor [rad/s]

Superscript
* : non-dimensional

2. Experimental apparatus

A schematic of the test model orientation, instrumentation, load and measurement system is shown in Fig. 1. The rotor consists of rotating components (blades and endplates) held by bearings in the side plates and in the upper support structure. The rotor was constructed from stainless steel mounted on a 10.0 mm diameter steel rod. One end of the rotor shaft is coupled to a pulley and to upper mounted load (powder brake) and torque meter by a timing belt on pulleys. We began the measurement from the unloaded state at the supply voltage of 0V to the powder brake and conducted the measurement by increasing the load until the rotor stopped.

The tests were carried out in the circuit water tunnel. The test section is illustrated in Fig.2. The test section is 0.6 m width, 0.5 m height and 3.0 m length with velocity variation in the empty tunnel up to ±1.5 %. The test section has a water surface like a field channel. The normal water level in the test section is set at H_0=0.4 m. No tunnel interference corrections are included. The coordinate system is chosen in such a manner that the origin is located at cross point between a plumb line suspended from the center of the rotor and

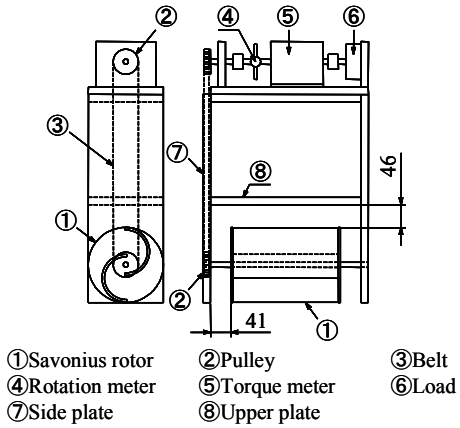

Fig. 1 Experimental apparatus

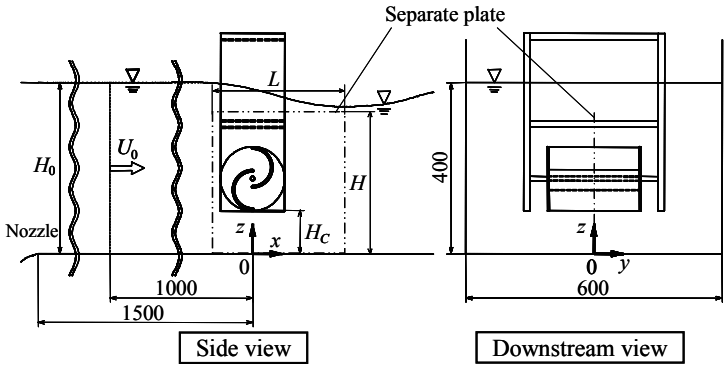

Fig. 2 Test section

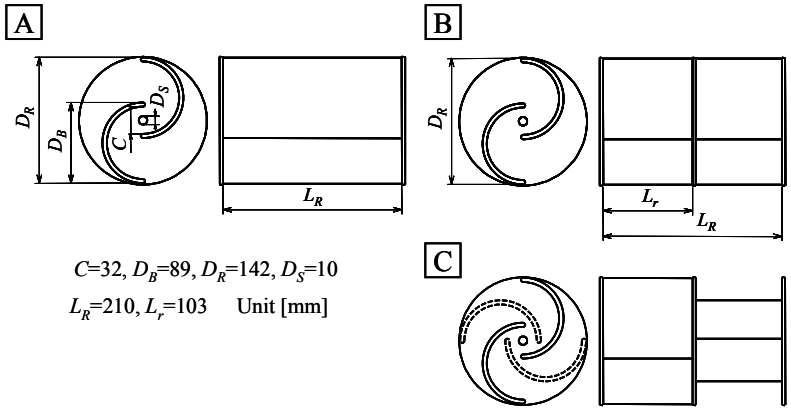

Type	Step	Phase difference [deg.]	Aspect ratio	Projected area A [m^2]	Overlap ratio C/D_B
A	single	–	L_R/D_B=2.4	0.03	0.36
B	double	0	L_R/D_B=2.4 L_r/D_B=1.2		
C		90			

Fig. 3 Savonius rotor specifications

bottom wall of the tunnel, the x-axis is along the flow direction, the y-axis is in the horizontal direction perpendicular to the flow, and the z-axis is in the depthwise direction. The distance between the rotor and the bottom wall of the tunnel is set at 100 mm, and is defined as H_C. The flow velocity at the center of the cross section at x=-1000 mm is U_0=0.8 m/s (constant) which corresponds to a Reynolds numbers ($Re=U_0 \cdot D_R/\nu$) of 1.1×10^5, where ν is a kinematic viscosity of water. The flow velocity distribution at this cross section is uniform except for the region near the wall in a tunnel.

For the experiment we used three types of Savonius rotors to evaluate the effect of the phase difference in the blades on the rotor's power performance. The each rotor configuration is shown in Fig. 3. All rotors' diameter, D_R, is 0.142 m and length, L_R, is 0.21 m. The blades are half cylinder with chord of D_B=0.089 m. The length of blade is L_R=0.21 m for Rotor A, and is L_r=0.103 m for Rotor C and B. The projected area of all rotors is 0.03 m^2, so that the rotor presented a water tunnel blockage of 12 %. Overlap of the two blades is C=0.032 m, the dimensionless overlap ratio C/D_B is 0.36. Rotor A is a standard Savonius rotor with two blades. Rotor B is the same as rotor A but has a 4mm-thick partition plate in the central section. Rotor C is the same as B but has a 90-degree phase difference in the blades between both sides of the partition plate. The table set below Fig. 3 shows the specification of each rotor. Rotors A and B have a different number of steps and Rotor B has a smaller aspect ratio. Rotor C has the same aspect ratio as B and is different from B only in the blade's phase difference. As indicated by the two-dotted line in Fig. 2, we conducted the experiment for the case with the separate plate attached to the central section of the rotor and evaluated the effect of the flow interaction at each step of the rotor. The separate plate was an aluminum flat plate of the height H=335 mm (H/D_R=2.4), length L=310 mm (L/D_R=2.2), and thickness t=2 mm. This specification was chosen to have appropriate length and height for the prevention of mutual interference of the flow field (including wake flow) around the rotor that was generated from each step of the double-step rotor. The rotation direction of the rotor is clock wise direction as shown in Fig. 2 when main flow direction is from left to right. A rotation angle of the blade chord is defined as θ which corresponds to the main flow direction is θ=0°. For Rotor C, θ is defined by the blade which locates in positive y-direction. A blade which located in the range $0° \leq \theta < 180°$ is named of advancing blade, located in the range $180° \leq \theta < 360°$ is named of returning blade.

3. Results and discussions

3.1. Measurement of power performance

Figure 4 shows the power performance of Rotors A, B and C illustrated in Fig. 3. The circle symbols present the result with Rotor A, the square ones the result with Rotor B, and the triangle ones the result with Rotor C. Open symbols show the results with the separate plate and solid ones the results without the separate plate. As can be seen from the graph, the curves have a peak (C_{Pmax}) at $\lambda \sim 1.1$ in all rotors. The rotational speed of rotors with separate plate were smaller than that of rotors without separate plate in a high rotational speed region ($\lambda > 1.25$). C_{Pmax} of Rotor B was approximately 15 % smaller than that of Rotor A, and smaller than the values measured under any other conditions. For Rotor B, no effect of the separate plate was observed on the power performance. It is indicated that no flow traverses the center section of Rotor B without the separate plate. Namely, without the phase difference in the blades, no interaction emerged in the flow field generated at each step of the double-step rotor. In other words, the decrease of C_{Pmax} of Rotor B should be attributed mainly to the reduction of the aspect ratio. Ushiyama, et al. reported the influence of the aspect ratio of Savonius wind rotors on these performance [3]. According to their report, the reduction of the aspect ratio decreased the rotation speed and suppressed the generation of the lift, causing the reduction of the torque. The decrease of C_{Pmax} of Rotor B could be caused for the same reason.

In comparing Rotor A and Rotor C, both without the separate plate, we found that C_{Pmax} was 10 % higher with Rotor C than A. Rotor C had a smaller aspect ratio than Rotor A, but had larger

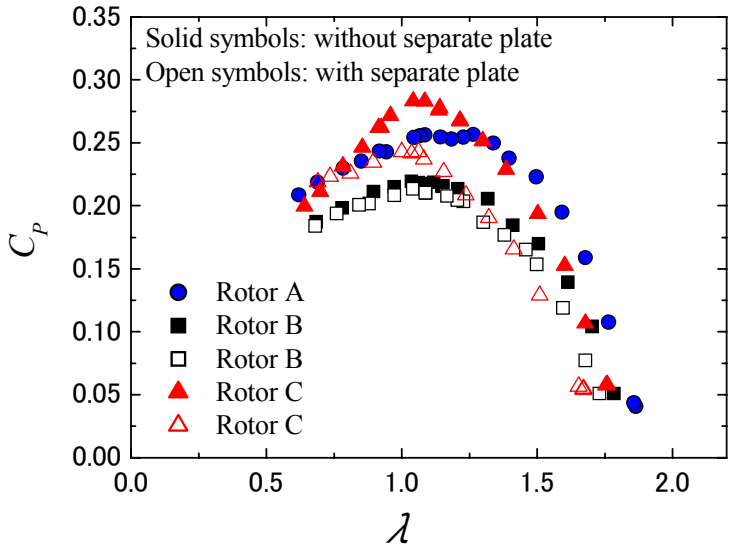

Fig. 4 Difference of power performance for rotor specifications

C_{Pmax}. Namely, the power performance enhancement due to the phase difference in the blades was larger than the power reduction due to the reduced aspect ratio. For Rotor C with the separate plate, C_{Pmax} significantly decreased by 14 %, compared to Rotor C without the separate plate. This indicates that the power performance enhancement due to the phase difference in the blades occurred only in the presence of the interaction in the flow from each step and the separate plate blocked the interaction. For λ>1.3, the power coefficient with Rotor A was larger than that with Rotor C. This seems to be because that the aspect ratio of Rotor A is larger than that of Rotor C. As a result, the rotational speed of Rotor A is higher than that of Rotor C.

The above measurement result of the power performance clarified that the flow interaction generated by the 90-degree phase difference in the blades was the main cause of the power performance enhancement of the phase difference rotor.

3.2. Flow visualization

To investigate the cause of the change in the power performance by the rotor types, we observed the flow field using the pigment streak-line method. For the pigment we used black ink used in fountain pens. The ink was slowly injected into the flow field through a pipe with an external diameter ϕ3.4 mm in order to avoid any influence on the rotor's characteristics. The injection point was set to x=-200 mm on the central section of rotor width. A clear acrylic rotor of the same shape as the one used for the power performance measurement was employed for the visualization test. As the experimental conditions, the tip speed ratio was λ~1.1 at which C_{Pmax} was obtained.

The results of the visualization are shown in Figs. 5(a) and (b). The ink was injected at the same height as the center of the rotation axis. In general, the flows around a standard type Savonius rotor are characterized as the following patterns. We therefore focused on these flow patterns.

(Ⅰ) Attached flow along the advancing blade's convex side
(Ⅱ) Dragging flow from the advancing blade's convex surface to the returning blade's concave side
(Ⅲ) Through-flow in the overlapping area
(Ⅳ) Flow from the upstream of the rotor to the returning blade's convex side

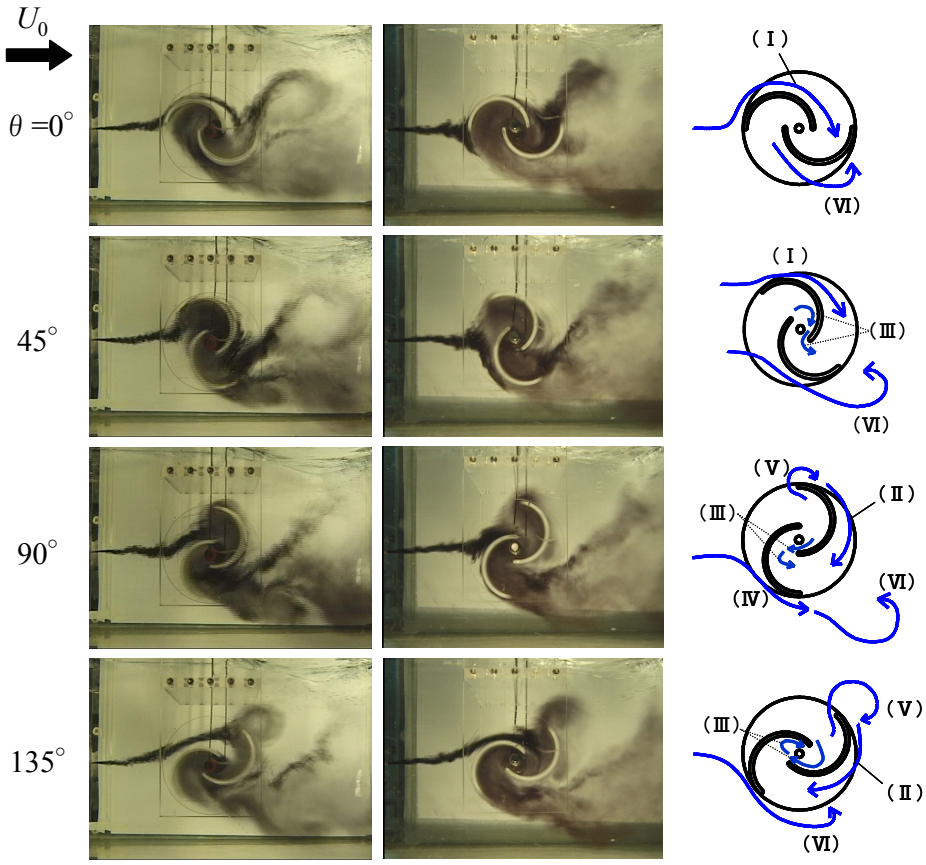

Fig. 5 Flow patterns from y-axial view

(Ⅴ) Shedding vortex from the advancing blade's tip
(Ⅵ) Shedding vortex from the returning blade's tip

Flow (I) produces a lift, (II) and (Ⅲ) restore the pressure on the returning blade's concave side, and (IV) affects the power reduction. Figure 5 (a) shows the result on the cross section at the center (y=0 mm) of Rotor A and Fig. 5 (b) the result on the cross section at the center of one of the steps (y=+50 mm) of Rotor C. The flow patterns of the two rotors look alike at any θ. The flow pattern model of the characteristic flow observed with the rotors is presented in the right side of Fig. 5 (b). The symbols assigned to the arrows in the figure correspond to (I) to (VI) mentioned above. With either rotor, the attached flow (I) was observed at $\theta \leq 45°$. This attached flow (I) became the dragging flow (II) toward the concave side of the returning blade. The former flow generates a lift and the latter restores the pressure on the concave side of the blade, both contributing to the enhancement of C_P. When the rotor with no phase difference was used, the attached flow (I) and dragging flow (II) were generated with a period of 180°. When the double-step rotor with the phase difference was used, on the other hand, the attached flow (I) and dragging flow (II) were generated with a period of 90° at the each step. The shedding vortex from the advancing blade's tip (V) was created with either rotor at θ=90°. Also the shedding vortex from the returning blade's tip (VI) was generated. At $\theta \geq 90°$, the shedding vortex (V) was separated from the advancing blade's tip and grew as flow to the downstream of the rotor. On the advancing blade's convex side, the flow was dragged to the returning blade's concave side (II). At the same time, the flow was stagnated on the returning blade's convex side (IV). The influence of the fluid drag due to the stagnation flow (IV) became larger than that of the

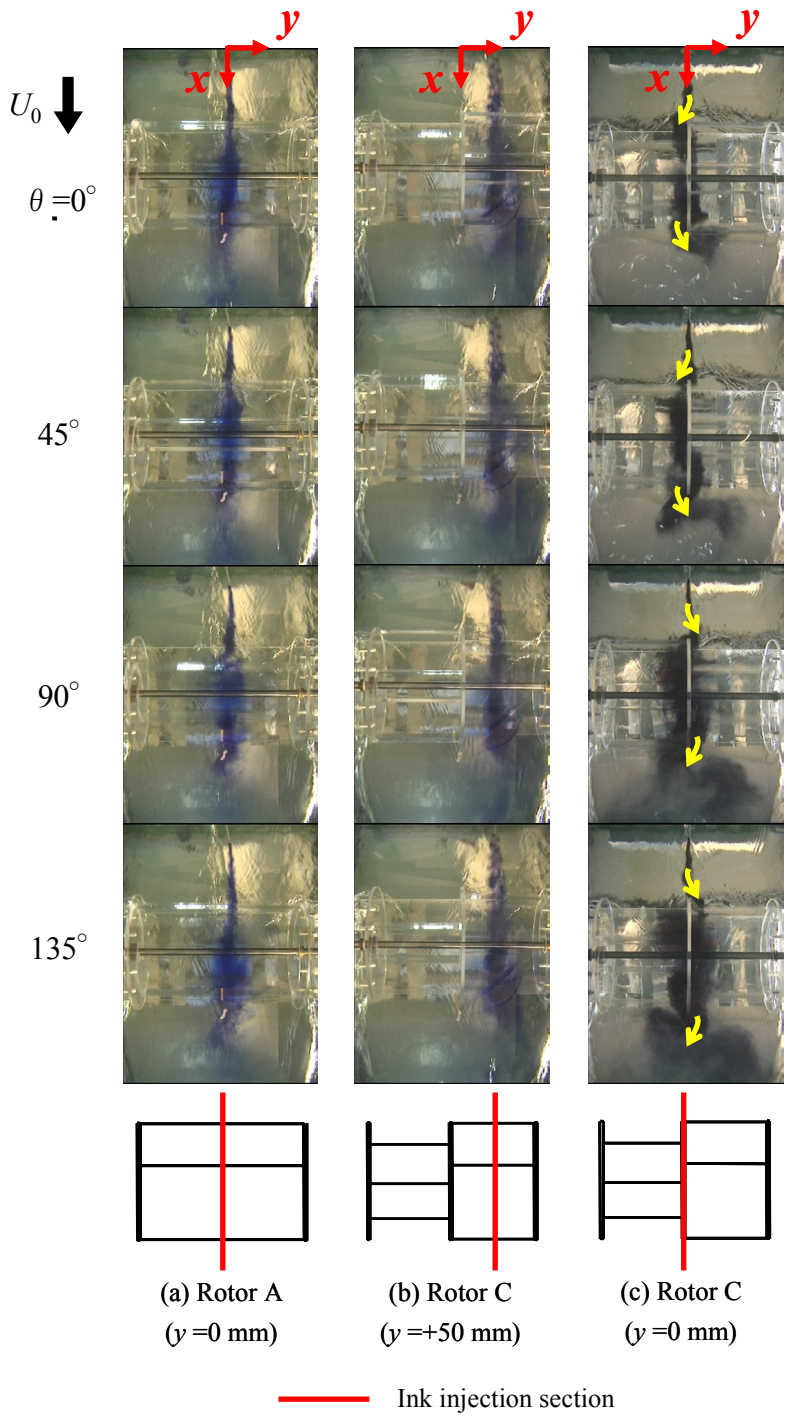

Fig. 6 Flow patterns from z-axial view

pressure restoration on the returning blade's concave side due to the dragging flow (II).

From the above results we can conclude that C_P with Rotor A with no phase difference in the blades decreases with the increase of θ. With Rotor C with the phase difference in the blades, at one of the steps, the increase of θ enhanced the fluid drag as with Rotor A, at the other step, the lift due to the attached flow (I) suppressed the decreasing of C_P.

Figure 6 shows flow patterns in Rotor A and Rotor C viewed from the z-direction. The ink was injected in plane with the central section of the one side step (y=+50 mm) as shown in Fig. 6 (b) and

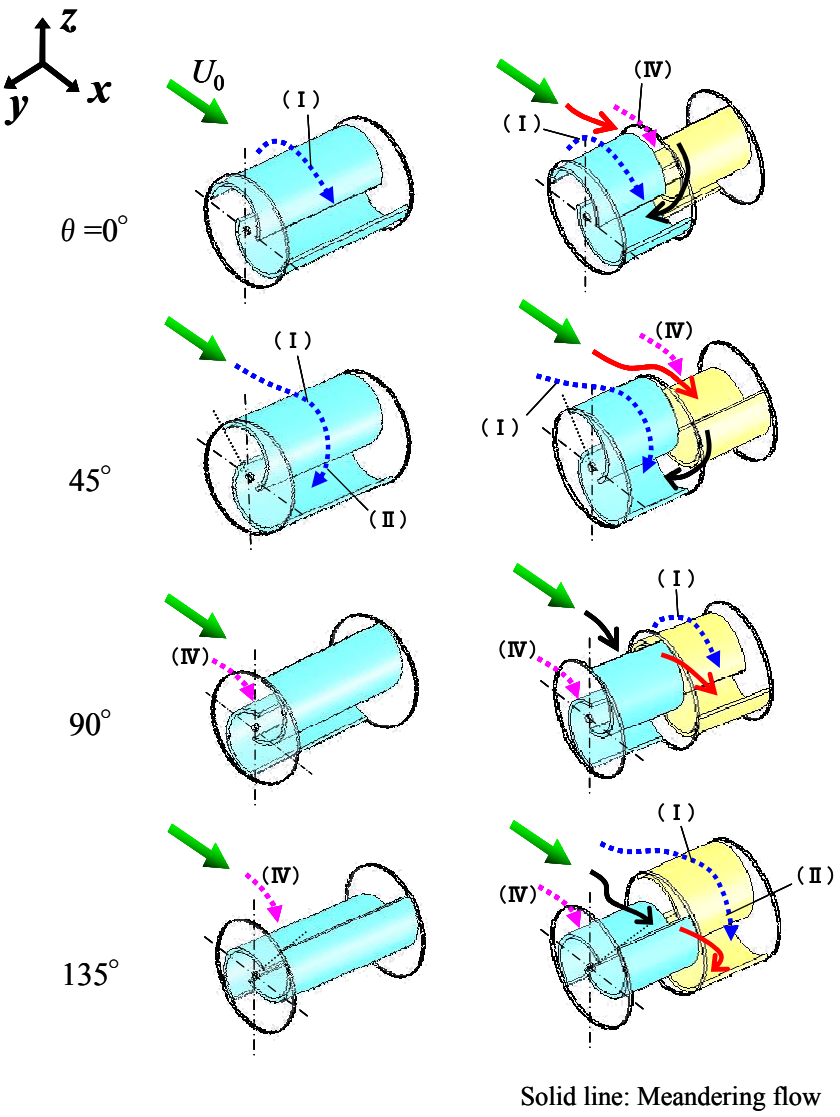

Fig. 7 Flow pattern models

with the center of the rotor (y=0 mm) as shown in Fig. 6 (c). It was observed for Rotor A that, at any θ, the ink injected from the upstream did not spread in the rotor axis direction (y-direction) and flew along the x-z cross section. This indicates the uniformity of the phenomena in the rotor axis direction.For Rotor C in Fig. 6 (b), the injected ink flew along the x-z cross section, as observed for Rotor A. It was found that the flow around the cross section (y=±50 mm) at the central section of each step of the double-step rotor was also two dimensional. Therefore the flow from the central section of each step did not interact. On the other hand, we observed the different flow in Fig. 6 (c) from that in Figs. 6 (a) or (b). The flow coming from the upstream to the center of the rotor flapped in the rotation axis direction as the rotor rotated. The meandering of the flow was synchronized with the rotation period of the rotor. The meandering flow into the rotor again flapped when going out into the downstream of the rotor, and the diffusion of the ink in the rotor's rotation axis direction was more significant than that in the other two cross sections. Figures 7 (a) and (b) shows the flow pattern models for Rotor A and Rotor C, created from the visualized results and the observation of the motion picture. The symbols assigned to the arrows in the figure correspond to the flow types mentioned above. The meandering flow to the step on the positive side of the y-axis is indicated by the black colored solid arrow and that to the step on the negative side is indicated by the red colored solid arrow. Flow in the y-direction was not observed at any rotational angle, so the flow was always

two-dimensional except for the region near rotor's end plates. On the other hand, with Rotor C that had the phase difference in the blades, we observed the periodically-meandering flow. When the ink injected in the upstream came into the rotor, it flapped in the rotor axis direction. In each step, the flow slanted toward the advancing blade whose angle was 135° from the main stream. The meandering behavior was repeated at a period of θ=90°. By the phase difference in the blades, the meandering flow generated in the upstream flow was sent to the advancing blade's concave side, enhancing the torque in the rotational direction. This could be one of the causes for the enhancement of C_P.

The meandering flow with a period of θ=90° in the rotation axis direction was also observed in the downstream tip of the rotor, as in the upstream tip. This was caused by the flow of the surrounding fluid to the low-pressure part of the returning blade's concave side which was tilted with an attitude angle of 45° from the main flow. The meandering flow in the back stream promoted the pressure restoration on the returning blade's concave side and enhanced C_P. The reduction of C_{Pmax} by the installation of the separate plate could be attributed to the meandering flow that suppressed the interactions between the flows from each step.

4. Conclusions

In the present study, we performed the experiment to investigate the influence of the 90-degree phase difference in the blades of the Savonius rotors on its power performance. From the measurement result of the power performance and the visualized results of the flow field inside and outside the rotor, we clarified the mechanism of the power performance enhancement of the double-step rotor with the phase difference in the blades. The following conclusions can be drawn:

(1) The 90-degree phase difference in the blades improved the power performance and enhanced the power coefficient by about 10 % at maximum.

(2) At the central cross section of each step of the double-step rotor with the phase difference in the blades, we found the flow pattern similar to that at the central cross section of the rotor with no phase difference. With the double-step rotor with the phase difference in the blades, a lift was generated with a period of θ=90° by the attached flow on the advancing blade's convex side, and the lift suppressed the power coefficient reduction due to the fluid drag on the returning blade's convex side on the other step. This was one of the major causes for the power coefficient enhancement of the double-step rotor with the phase difference in the blades.

(3) The double-step rotor with the phase difference in the blades created the meandering flow in the central cross section in both the upstream and downstream tip of the rotor. The meandering flow had an influence with a period of θ=90° on each step of the rotor, causing the rotational torque enhancement of the advancing blade's concave side and the pressure restoration of the returning blade's concave side.

Acknowledgement

This work was supported partly by the Grant-in-Aid for Exploratory Research under Grant No.19651033 from Japan Society for the Promotion of Science.

References

(1) Sheldahl, R. E., Feltz, L. V. and Blackwell, B. F., Wind Tunnel Performance Data for Two and Three-Bucket Savonius Rotors, *Journal of Energy*, Vol. 2, No. 3 (1978), pp. 160-164.

(2) Sivasegaram, S., Secondary Parameters Affecting the Performance of Resestance-type Vertical-axis Wind Rotors, *Wind Engineering*, Vol. 2, No. 1 (1978), pp. 49-59.

(3) Ushiyama, I., Nagai, H. and Shinoda, J., Experimentally Determining the Optimum Design Configuration for Savonius Rotors, *Transactions of the Japan Society of Mechanical Engineering*, *Series B*, Vol. 52, No. 480 (1986), pp. 2973-2981.

(4) Bergeles, G. and Athanassiadis, N., On the Field around a Savonius Rotors, *Wind Engineering*, Vol. 6, No. 3 (1982), pp. 140-148.

(5) Murai, H., Kataoka, M., Narasaka, T., Watanabe, H. and Onuma, S., Influence of Flaps and Deflectors on Power and Torque Characteristics of Savonius Rotor, *Journal of the Visualization Society of Japan*, 4-Suppl. (1984), pp. 11-16.
(6) Fujisawa, N., Shirai, H. and Saikawa, Y., Investigation of the Field and Power Mechanism of a Savonius Rotor: Flow Visualization by a Smoke-wire Method, *Transactions of the Japan Society of Mechanical Engineering*, *Series B*, Vol. 53, No. 496 (1987), pp. 3716-3721.
(7) Oagawa,T., Research of a Savonius Rotor: Part 1 Theoretical Analysis, *Transactions of the Japan Society of Mechanical Engineering*, *Series B*, Vol. 49, No. 441 (1983), pp. 976-984.
(8) Ishimatsu, K., Shinohara, T. and Takuma, F., Numerical Simulation for Savonius Rotors : Running Performance and Flow Field, *Transactions of the Japan Society of Mechanical Engineering*, *Series B*, Vol. 60, No. 569 (1994), pp. 154-160.
(9) Sivasegaram, S., Concentration Augmentation of Power in a Savonius-Type Wind Rotor, *Wind Enginnering*, Vol. 3, No. 1 (1979), pp. 52-61.
(10) Sabzavari, A., Performance Characteristics of Concentrator-Augmented Savonius Wind Rotors, *Wind Engineering*, Vol. 1, No. 3 (1977), pp. 198-206.
(11) Ueno, H., Mino, M. and Takada, N., Savonius type wind turbine (The influence of wind concentrator), *Journal of Japan Solar Energy Society*, Vol. 30, No. 5 (2004), pp. 35-40.
(12) Ogawa, T., Tahara, K. and Suzuki, N., Study on a Savonius-Type Wind Turbine: 2nd Report, Effects of Guide Vanes, *Transactions of the Japan Society of Mechanical Engineering*, *Series B*, Vol. 51, No. 471 (1985), pp. 3516-3522.
(13) Sato, S., Kikuchi, K. and Ushiyama, I., An Experimental Study on Power Augmentation of Savonius Rotor, *Proceedings of JSES/JWEA Joint Conference*, Vol. 1997, (1997), pp. 197-200.
(14) Lei, W., Kitani, O., Okamoto, T. and Torii, T., Experimental Study on the Efficiency Increase of a Savonius Windmill (Part 1): Test of Concentrator's Performance, *Journal of the Japanese Society of Agricultural Machinery*, Vol. 58, No. 2 (1996), pp. 11-17.
(15) Savonius, S. J., The S-Rotor and Its Applications, *Mechanical Engineering*, Vol. 53, No. 5 (1931), pp. 333-338.
(16) Takaku, A. and Ogawa, Y., Practical Application of Multi-Step Vertical-axis Wind Rotor (2nd Report, Characteristics of the Third Wind Rotor) (in Japanese), *Turbomachinery*, Vol. 13, No. 12 (1985), pp. 711-721.
(17) Khan, M. H., Model and Prototype Performance Characteristics of Savonius Rotor Windmill, *Wind Engineering*, Vol. 2, No. 2 (1978), pp. 75-85.
(18) Hayashi, T., Li, Yan. and Hara, Y., Wind Tunnel Tests on a Different Phase Three-Stage Savonius Rotor (<Special Issue> Experimental Mechanics in Heat and Fluid Flow), *JSME International Journal*. *Series B*, *Fluids and thermal engineering*, Vol. 48, No. 1 (2005), pp. 9-16.
(19) Menet, J. L., A double-step Savonius rotor for local production of electricity: a design study, *Renewable energy*, Vol. 29, (2004), pp. 1843-1862.
(20) Suzuki, S., Kato, E. and Tachikawa, T., Flow in the vicinity of vane of Twist Savonius Rotor, *Ibaraki district conference*, Vol. 2005, (2005), pp. 137-138.
(21) Higo,T., Takasugi, Y., Fujiwara, T. and Noguchi, H., Efficiency of Savonius Hydro Turbine for Tidal Currnet, *Reports of the Government Industrial Research Institute Chugoku*, No. 32 (1989), pp. 1-13.
(22) Tan, S., Shimizu, Y. and Kikuyama, K., Experimental Studies on a Savonius Rotor with Casing, *Transactions of the Japan Society of Mechanical Engineering*, *Series B*, Vol. 63, No. 611 (1997), pp. 2356-2363.
(23) Okuda, K., Watabe, T., Kondoh, H. and Yano, K., Study of the Wave Energy Conversion System Fixed on the Seashore: Part 1 A Water Turbine of Savonius Type for Wave Power, *Memoirs of the Muroran Insutitute of Technology*, (1981), pp. 427-432.